Physics Procedia

Volume 75, 2015, Pages 314–325

20th International Conference on Magnetism

Imaging of Condensed Quantum States in the Quantum Hall Effect Regime

Josef Oswald[1] and Rudolf A. Römer[2]

[1]*Institute of Physics, Leoben University, Franz Josef Str. 18, A-8700 Leoben, Austria*

[2]*Department of Physics and Centre for Scientific Computing, University of Warwick, Coventry CV4 7AL, UK*

josef.oswald@unileoben.ac.at, R.Roemer@warwick.ac.uk

Abstract

It has been proposed already some time ago that Wigner crystallization in the tails of the Landau levels may play an important role in the quantum Hall regime. Here we use numerical simulations for modelling condensed quantum states and propose real space imaging of such highly correlated electron states by scanning gate microscopy (SGM). The ingredients for our modelling are a many particle model that combines a self-consistent Hartree-Fock calculation for the steady state with a non-equilibrium network model for the electron transport.

If there exist condensed many particle quantum states in our electronic model system, our simulations demonstrate that the response pattern of the total sample current as a function of the SGM tip position delivers detailed information about the geometry of the underlying quantum state. For the case of a ring shaped dot potential in the few electron limit it is possible to find regimes with a rigid (condensed) charge distribution in the ring, where the SGM pattern corresponds to the probability density of the quantum states. The existence of the SGM image can be interpreted as the manifestation of an electron solid, since the pattern generation of the charge distribution requires certain stability against the moving tip potential.

Keywords: Wigner crystallization, Hartree-Fock calculation, quantum Hall regime, network model, scanning gate microscopy

1 Introduction

During the last decade scanning gate microscopy (SGM) has gained attention because of its assumed non-invasive character for investigating quantum coherent phenomena [1,2,3,4,5,6,7,8]. The most common output from SGM experiments are conductance maps. These are maps of the total device conductance as a function of the gate tip position. In these experiments, the gate tip provides a local distortion of the electron system and the response of the device as a whole, e.g. the total device current, is recorded. This local distortion does not destroy the quantum phase of

Selection and peer-review under responsibility of the Scientific Programme Committee of ICM 2015

doi:10.1016/j.phpro.2015.12.038

the system and allows monitoring phase coherent quantum states in transport. SGM is therefore an indirect measurement method, which nevertheless allows constructing amazingly detailed real space maps of wave functions and interference patterns [9,10,11,12,13]. Since this method always creates 2D images, the term 'imaging' has been used quite generously in context with this experimental method. However, in most cases these images are indications of a number of different effects, but they only rarely have to do with real space images of the involved quantum states. So far most SGM experiments have been performed on almost macroscopic length scales with scan regions of the order of several microns. An early kind of SGM experiments has been performed by Baumgartner et al [14]. In these experiments the tip potential acts more or less as a local classical gate control of the modulation of the saddle potentials in the landscape of random potential fluctuations in the quantum Hall regime. If potential saddles are close to becoming insulating, like in the case of the quantum Hall plateau transition regimes, the tip causes a strong response if it hits such a saddle. In this way Baumgartner et al demonstrated, that close to the transition regime of the integer quantum Hall effect (IQHE) only very few or even single saddles are involved, that act as so called hot spots in the quantum Hall plateau transition regime. However, this kind of experiments is more likely a method for localizing critical potential saddles (hot spots) but it cannot yet be classified as direct imaging of current flow or imaging of quantum states. More recent experiments of similar type have been done by Paradiso et al [15]. The authors investigated back scattering by impurity-induced anti-dots in quantum Hall restrictions. The main observation is an arc structure in the SGM image that is centered at the anti-dots. Either Aharanov-Bohm (AB) oscillations and/or charging effects that are driven by the tail of the moving tip potential, acting on the anti-dot, have been identified as the origin of this fine structure. The arc geometry of the oscillations in the SGM image consists of all tip positions that create the same potential distortion at the anti-dot. Another experiment by the same authors aims at imaging of fractional incompressible stripes in integer quantum Hall systems [16]. The main role of the tip potential in this case is to create alternating compressible and incompressible stripes by variation of the tip potential at the QPC, which happens by moving the tip towards or away from the QPC saddle. As a consequence the image results mainly from the dependence of the tip potential at the QPC as a function of tip position. In this way the authors have obtained the important result that also fractional stripes can be found in the QPC even in the integer regime of the host electronic system. That means that the tip drives the electron systems locally into the fractional regime while the system as a whole remains in the integer regime. However, the obtained images are not real space images of those stripes. A small selection of some more experiments of this kind by other authors can be found in Refs. 5, 8, 17, 18, 19 and 20.

A different class of SGM experiments that has become dominating by now is directed towards probing of current flow in the ballistic regime. The main effect of the tip potential by now is that it becomes a scatterer for the electron waves. One major result is the observation of fringes in the SGM images that can be attributed to interference effects between different electron paths that include elastic scattering at the moving tip. Depending on the interplay of the tip with the confinement of the electronic device this can change the mode structure for transport of e.g. an open quantum stadium as a whole. This is demonstrated in a recent SGM experiment in the ballistic regime of a quantum stadium with constrictions at both sides [21]. The fine structure of the patterns is consequently interference driven and also not yet a direct real space image of the involved quantum states, although this delivers already substantial information about the geometry of the involved quantum channels. A lot of work of this type can be found in the literature by many different authors and a limited selection can be found in Refs 7, 11, 12, 22, 23, 24, 25, 26 that spread over several years.

On this background the direct real space imaging of quantum states seems to remain the ultimate goal of the SGM method. At this point we arrive at the same time at the very fundamental question if it is possible at all to use (non-equilibrium) transport in order to probe (equilibrium) Eigenstates. There already can be found a few approaches to real space imaging in the past. A proposal of that kind was made by Boyd et al, which suggests probing the localized quantum states of a quantum dot, by

mapping the coulomb blockade potential as a function of tip position within the dot [27]. That proposal is based on theoretical investigations that demonstrate that the modification of the coulomb blockade potential by the SGM tip depends on the probability density of the electronic state at the actual tip position. However, this proposal has been made for very special considerations like an almost linear dot which is created from a quantum wire by pinch-off and a modeling based on non-interacting single electron states. Another already much earlier approach deals with quantum rings, where the authors claim direct imaging of quantum states. The modelling is based again on the single electron picture at the Fermi level at vanishing magnetic field [3]. An overview on SGM on semiconductor nanostructures by 2010 is given also in Refs.28 and 29.

Concerning modelling there are a number of theoretical approaches to the SGM method, but most of them are developed for zero or weak magnetic fields and are addressing directly the current flow. Besides those papers that are included already in the references above, recent and quite sophisticated theoretical work in this context has been done by Gorini et al [30] and Chwiej et al [31] that assume hard wall confinement and zero magnetic field, while screening of the tip potential has been considered based on a previous study [22]. However, despite different methods of incorporating confinement and screening, the major focus is always directed at scattering of Fermi edge electrons, that means that the substantial many particle character of the electron system is neglected, while that plays an important role if aiming at condensed electron states, like we do in this paper.

For achieving our goal of direct real space imaging of quantum states, we have to look for an electronic system with strongly reduced scattering. In order to preserve the many body character of the Eigenstates the object for imaging should additionally be somehow separated from the still experimentally required non-equilibrium current transport. We need also a system that is able to provide rigid (condensed) quantum states that have certain stability against probing. In this context the quantum Hall effect (QHE) regime appears as a suitable candidate because back scattering is strongly suppressed and there also co-exist localized and de-localized states. It has been already proposed earlier, that Wigner crystallization might be present in the tails of the LLs (see e.g. Ref.32). Picking up the idea of magnetic field induced Wigner crystallization, we can expect that the QHE regime provides such condensed quantum states in the vicinity of magnetic field driven metal-insulator transition at low Fermi wave vectors that should be possible to be imaged in real space by SGM. For this purpose we need a mechanism that transfers the information from localized states to the states that maintain non-equilibrium current transport. Since in this case we are not interested in observing quantum coherence in ballistic non-equilibrium transport itself, quantum coherence in the transport model is not explicitly needed. However, screening depends sensitively on the charge distribution that in turn depends on all aspects of the involved quantum states. Therefore we expect that any impact even on condensed quantum states by e.g. the moving SGM tip will affect the screened potential. A nearby potential saddle of a QPC that is tuned to the tunneling regime then will produce a response not only when hitting this saddle directly by the moving tip (like in the experiments of Baumgartner et al in Ref.14), but also if the tip hits a condensed nearby quantum state. Therefore the response pattern may provide information also about the lateral distribution of the probability density of involved condensed quantum states, even if they are not directly carrying current.

In this paper we will demonstrate by numerical simulations, that such real space imaging of condensed quantum states by the SGM method is indeed possible. Our ingredients are a many particle model for the steady state, that is achieved by a self-consistent Hartree-Fock calculation and for the transport we use the non-equilibrium network model as outlined in the next paragraph.

2 Model

The equilibrium steady state for the disordered many particle electronic system is calculated by the Hartree-Fock approximation using directly the method of Sohrmann and Roemer [33,34]. A detailed

description of the non-equilibrium network model (NNM) for current transport can be found in [35, 36], while in Ref. 37 among others, there is a summary of both, the HF-approach and the NNM. Since the NNM is a more recent development and thus not so well known like the Hartree-Fock approach, a very short summary of the NNM will also be given below.

The main physical basis of the QHE regime is the existence of long range potential fluctuations. Magnetic bound states (internal edge channel loops) are created, which follow the contours of the random potential and their position on the energy scale is determined by the Fermi energy. Transport across the bulk in the transition regime between QH plateaus is possible, if such loops meet at the saddle energy or if tunneling across the saddle is sufficient to allow current flow across the bulk. The main ingredient of the NNM is that the excitation potential (electro chemical potential μ), which has a non-uniform lateral distribution for the non-equilibrium case, is transmitted by the nodes (see Fig.1a) of the network as:

$$\begin{pmatrix} \mu_2 \\ \mu_4 \end{pmatrix} = \begin{pmatrix} T & R \\ R & T \end{pmatrix} \begin{pmatrix} \mu_1 \\ \mu_3 \end{pmatrix}$$

The transmission and reflection probabilities T and R are related to a function P as follows:

$$P = \frac{R}{T} \qquad \text{with} \qquad P(x,y) = \exp\left[\frac{-L^2 \cdot E_F(x,y)}{eV} \cdot \frac{eB}{h} \right]$$

E_F is the Fermi energy relative to the local saddle energy at grid position *(x,y), L* and *V* can be roughly understood as the representative period and amplitude of the potential fluctuations. In particular *L* is the period and *V* the amplitude of a two-dimensional cosine function, which has the same second order Taylor expansion like the actual native saddle potentials. Therefore parameter pair *L* and *V* serves finally as a parameterization of the typical saddle curvature [38]. Fig.1a-c shows schematically, how the grid of the network is built from interconnecting a number of nodes. Four adjacent nodes represent a loop (Fig.1b), while these loops are connected to further loops by tunneling junctions that are represented again by the nodes (Fig.1c). Therefore parameter pair *L* and *V* serves finally as a parameterization of the typical saddle curvature [42].

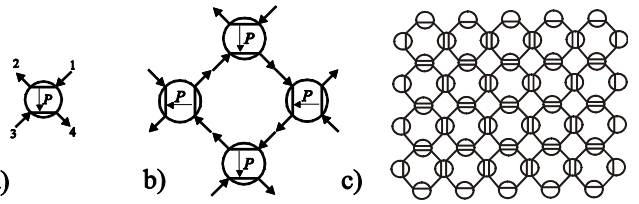

Figure 1: a) Network symbol for a single potential saddle, which becomes a node of the network model, b) network for a single magnetic bound state created by 4 nodes, c) a complete network is created by a periodic continuation of such loop elements.

Including an additional long range disorder potential, the saddle energies get non-uniformly distributed and a partly transmission and reflection at the nodes appears only at those locations where the saddle energy gets close to the Fermi energy. This usually happens only for a small fraction of the nodes in the network, like indicated schematically in Fig.2. All nodes (saddles) with energy far from the Fermi energy have either full transmission (*T=1, R=0*) or full reflection (*T=0, R=1*), depending on whether the Fermi energy is above or below the saddle energy. In this way the network guides the

channels around potential fluctuations and only those nodes at which the saddle energy gets close to the Fermi energy become physically active (red arrows in Fig.2). In this way the NNM approximates arbitrarily shaped magnetic bound states and also finds the "hot spots" (active saddles of the disordered potential). Also without using the HF calculations this network model had been successfully used to obtain e.g. average microscopic details of a disordered QH system [38]. The application of this network model is substantially extended by combining it with the self-consistent many body Hartree-Fock calculation for obtaining the screened potential landscape, which determines the details of the loops and the tunneling junctions that are handled by the NNM.

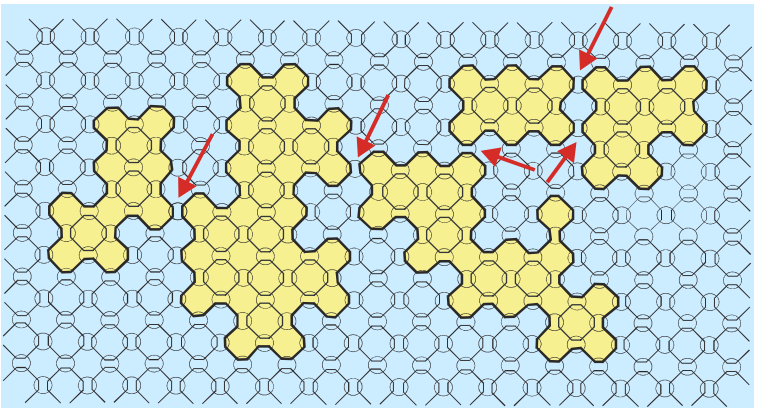

Figure 2: Schematic network representation of magnetic bound states that are created by a smooth long range disorder potential. The bold lines follow the transmission of the nodes and in this way resemble the random magnetic bound states. The active saddles for transport become those nodes of the network where such magnetic bound states get close to each other and allowing current flow by tunneling (indicated by red arrows).

Our non-equilibrium network model (NNM) [35, 37] addresses continuous dissipative current flow in a network of disordered saddle potentials [39]. One of the main points in this paper is to include screening into the NNM, i.e. the main effect of the many-body interactions [40]. This problem has been already addressed by Römer et al [34, 33, 41,42], using a Hartree-Fock calculation to get the self-consistent solution for the screened potential and the percolating wave functions. However, this is a steady state solution, which does not carry any injected current, unlike in the NMM and, of course, in experiments. One frequently used approach is to calculate the Kubo conductivity or mapping the probability flow to a conductance by applying the Landauer formula [3, 11, 22, 26, 30]. However, this still is not a direct modelling of dissipative excess current flow. Our NNM is a fundamentally different approach that provides a solution for the lateral non-equilibrium distribution of the introduced electrochemical potentials, and which does not make use of the Landauer formula at all. Results of this new approach are presented in the next paragraph that deals with modeling of scanning gate microscopy experiments. One major requirement for the Hartree-Fock model is to account for a soft Fermi edge for the occupation of the quantum states. Another requirement is introducing a predefined fixed Fermi energy instead of using a fixed number of electrons. The latter results from the fact, that in reality the electronic systems are embedded in a 2DEG reservoir that pins the Fermi level according to the filling of the Landau levels in the bulk region. This causes electrons to move in and out of the dot structure depending on the magnetic field dependent Fermi level in the bulk. However, a back gate in real structures will care for keeping the charge neutrality in the dot region and therefore charge neutrality is also assumed in our model even while the electron number changes in the dot region at different magnetic fields. Details will be published elsewhere and we now turn to the results of our model.

3 Results and Discussion

For demonstration we use here an idealized model system and Fig. 3 shows a contour plot of the bare potential that defines a ring shaped confinement. The model potential is created by the superposition of 4 repulsive Gaussian peaks that are arranged in a square with the maxima recognizable as red colored. The overlap of these Gaussian peaks forms the saddles of the quantum point contacts (QPC), while in the middle a pronounced potential minimum is created. In order to compose the ring shape, another narrow repulsive Gaussian peak is placed in the middle, leaving a ring shaped potential minimum that can be recognized in blue color.

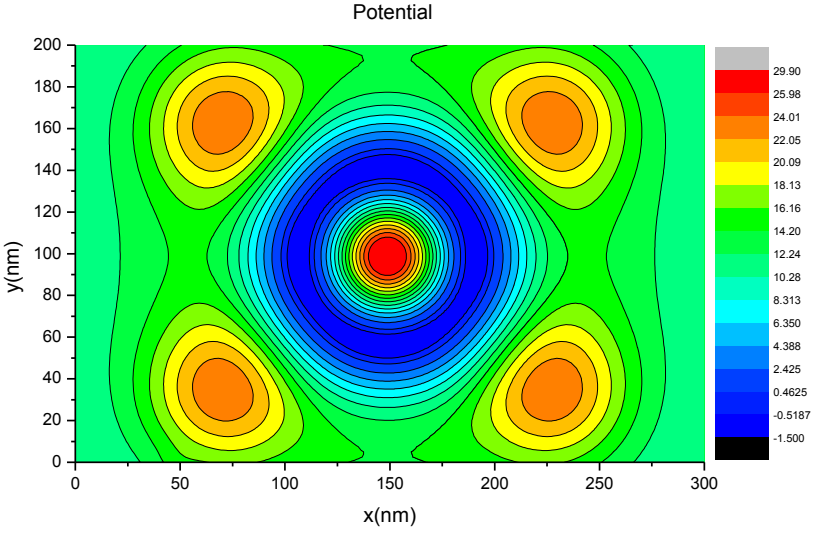

Figure 3: Contour plot of the bare ring shaped confinement potential with a diameter of about 100nm and a depth of about 15 meV as compared to the saddle energies of the QPCs.

For the calculation a constant magnetic field of B=2.5 Tesla was used and the Fermi energy was chosen in a way that a total of 8 electrons appear in the potential ring, while at the same time in the NNM these saddles appear in the tunneling regime. For the ongoing calculation the Fermi energy was kept constant in order to account for the situation of a real electronic structure where the Fermi level gets pinned outside in the reservoir of the surrounding two-dimensional electron gas of the bulk.

The current has been supplied to contacts at the left and right boundary and the total device current has been calculated by the NNM. This current passes the saddles on the left and right of the opening as a tunneling current. The charge distribution inside the ring affects the tunneling barriers and thus the total sample current sensitively responds to any modifications of the charge distribution in the ring by the scanning gate tip. Fig. 4 shows the charge distribution while the SGM tip is outside the ring where it is not affecting the electronic state. It is clearly seen, that the charge distribution appears along the ring shaped minimum, with a tendency of charge accumulation in front of the QPCs at left and right. We see only 6 charge maxima while there are 8 electrons in the system, which is a result of the many particle character of the wave function, where the electrons lose their individuality and therefore must not be attributed to individual charge maxima.

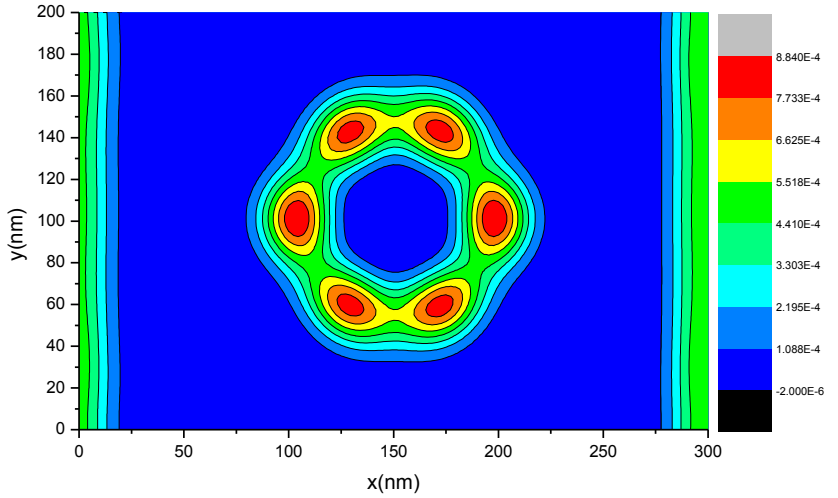

Figure 4: Contour plot of the charge distribution obtained from the Hartree-Fock calculation in arbitrary units for a magnetic field of B=2.5 Tesla. In this regime the electron system appears fully spin polarized.

Fig.5 shows a contour plot of the two-point sample conductance as a function of the SGM tip position in multiples of the universal conductance. The scan range was chosen in the longitudinal direction between x = 50 and 250nm and in transverse direction between y = 0 and 200nm in steps of 5nm. From the color scale one can see, that the total conductance is reduced by up to 10% if the SGM tip hits the positions of the maxima of the undisturbed charge density and that the complete pattern nicely resembles the original charge distribution.

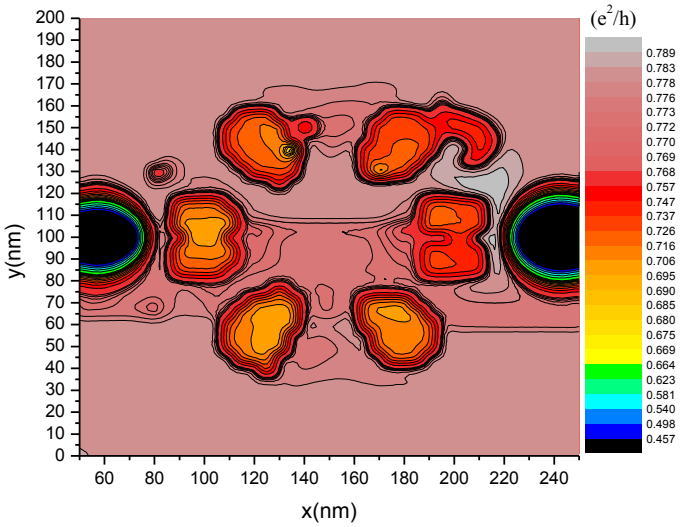

Figure 5: SGM response pattern as a contour plot of the two-point conductance (in multiples of e^2/h) as a function of SGM tip position. Tip parameters: circular Gaussian shape of repulsive height 1mV and half width diameter of 20nm.

The fact, that the contrast of the image does not depend whether the SGM tip hits a charge maximum close to or far from the active saddles indicates that we are indeed dealing with a non-local quantum state, where there are no individual electrons arranged along the ring. Classical coulomb interaction based on the single electron picture can therefore clearly be ruled out as the driving mechanism in this system. The dark circular spots on the left and right are caused by classical pinch-off where the SGM tip directly hits the active saddles (like in the Baumgartner experiments of Ref.14), which also proofs that the main features of the response pattern do not result from classical coulomb effects. In order to clarify the mechanism that leads to the above images, the following series of figures will show the charge distribution for situations, where the SGM tip hits the quantum state at different locations. The first of this series is Fig. 6, which shows the charge distribution if the SGM tip hits exactly the lower left maximum of the undisturbed charge distribution at x=120nm and y=60nm.

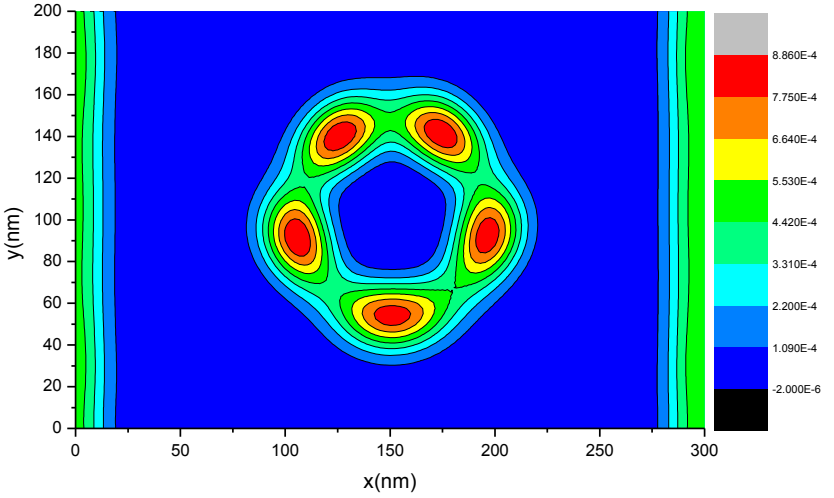

Figure 6: Contour plot of the charge distribution for a position of the SGM tip at x=120nm and y=60nm.

From Fig.6 one can see, that the charge distribution gets changed now by the action of the tip that leads mainly to the disappearance of one charge maximum, while the system still seems to try to keep some kind symmetry. This leads on one hand to the disappearance of charge at the actual tip position; on the other hand the changed overall arrangement also removes some of the charge that had been accumulated in front of the left and right QPC. From this fact we can understand, that the screening of the saddle potential gets reduced, which consequently also reduces the tunneling current, as it appears in the SGM pattern.

It is important to note that the total number of 8 electrons in the dot remains unchanged in this situation. Fig.7 shows the charge distribution for the case that the SGM tip hits the undisturbed charge maximum in front of the left QPC. In this position the tip suppresses the charge maximum in front of the QPC and consequently reduces screening of that saddle, which reduces also the tunneling current. It is important to note, that the tunneling current first increases again if the tip moves further towards the QPC, although the tip itself is repulsive. This again demonstrates that the mechanism is not a trivial classical coulomb effect. However, if the tip finally reaches the saddle of the QPC, it leads to a pure classical pinch-off as indicated by the black circular spots in Fig. 5. The opposite QPC on the right might even open up because of the further charge accumulation, but since it is connected in series with current path this does not show up in the response and only the decrease of the current due to the left QPC dominates the pattern.

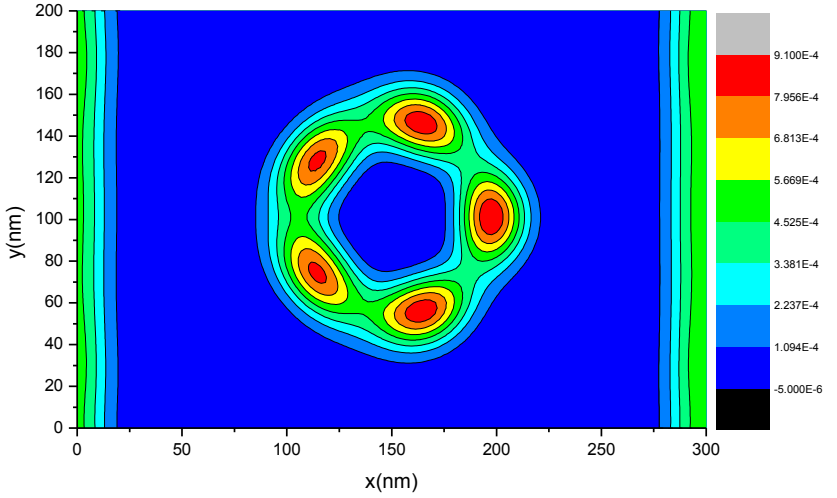

Figure 7: Contour plot of the charge distribution for the SGM tip is at the position of the undisturbed charge maximum that is right in front of the left QPC at x=100nm and y=100nm.

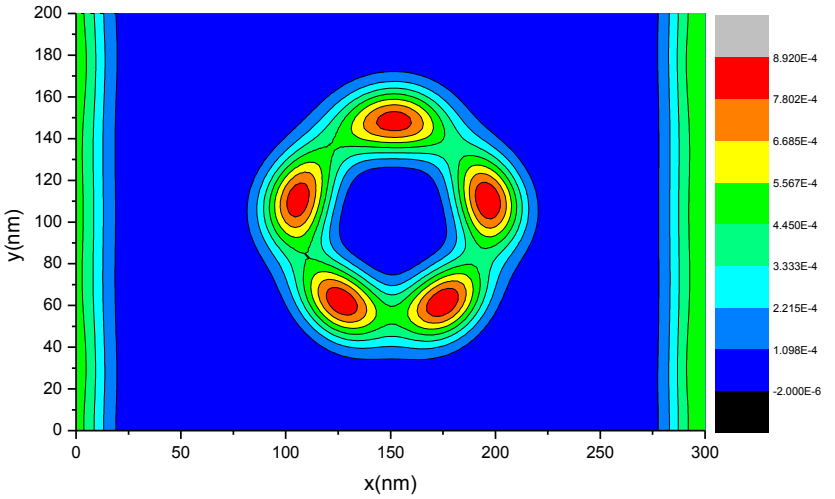

Figure 8: Contour plot of the charge distribution for the SGM tip is at the position of the upper right undisturbed charge maximum at x=180nm and y=140nm.

Fig.8 shows a situation equivalent to Fig.6, but this time the SGM tip is hitting the upper right undisturbed charge maximum. The effect is the same and the charge is pushed away from the tip by reducing to 5 charge maxima (while leaving the number of 8 electrons constant) which again removes some charge from the QPCs. Considering the overall behavior, it is interesting to note that although the SGM tip significantly modifies the charge configuration, the response pattern reflects the undisturbed charge distribution. On this background it is an interesting question, if this strong impact

of the tip on the charge distribution is really needed in order to get a SGM response at all. For this purpose the same simulation but with an extremely weak tip potential of only 0.1mV was used. We checked that this weak tip potential does not cause significant charge redistribution even if placed at the positions of Figs. 6-8 (not shown). However, investigating the response pattern, we still find a well pronounced, of course much weaker SGM response still reflecting the geometry of the undisturbed charge distribution (see Fig. 9). Experimentally such a weak response could be investigated using Lock-in technique for the tip potential modulation. While the overall SGM pattern nicely reflects the charge distribution, the physical background of further details of the images is the goal of ongoing and future investigations.

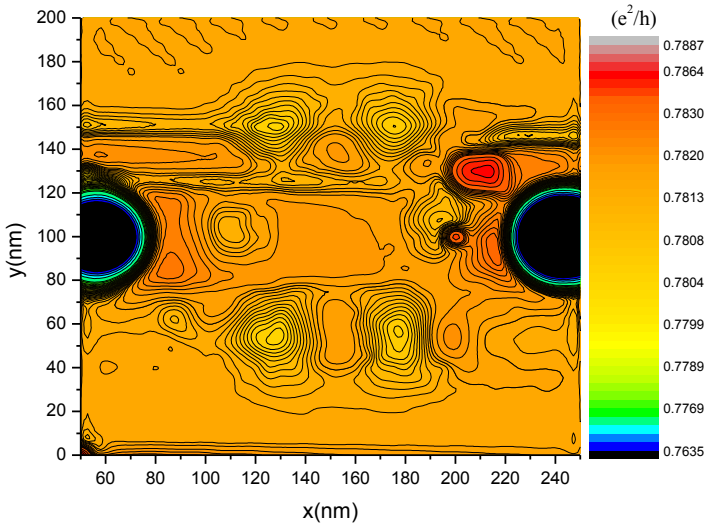

Figure 9: SGM response pattern as a contour plot of the two-point conductance (in multiples of e^2/h) as a function of SGM tip position. Tip parameters: circular Gaussian shape of repulsive height 0.1mV and half width diameter of 20nm.

4 Summary

We have introduced a numerical method to study magneto transport in the quantum Hall regime. The screening effects of the electron system are treated on the basis of a many particle Hartree-Fock approximation. The in real experiments present non-equilibrium current transport is addressed within a non-equilibrium network model (NNM), that uses the screened potential of the Hartree-Fock model for calculating the lateral distribution of the experimentally injected current. In this way the injected current monitors effects that are going on in the underlying electron system, like e.g. the impact of a moving gate tip. In this paper we have applied this model to scanning gate microscopy and have demonstrated that this experimental method provides the potential to image condensed many particle quantum states, like e.g. Wigner crystals.

We used a model system that represents a ring shaped confinement potential of about 100nm diameter and 15mV depth, that is filled with 8 fully spin polarized electrons. The undisturbed many particle quantum state exhibits 6 maxima in the charge distribution that are regularly arranged in the potential ring. The maxima of the charge distribution appear pinned in front of the potential saddles of quantum point contacts that open the ring to the environment. That charge distribution has some

stability against the action of a tip potential and thus can be interpreted as Wigner crystallization in this very special model system. If the tip potential is strong enough (repulsive Gaussian of about 1mV height and 20nm half width diameter), it is able to suppress one of the charge maxima if located right at the position of one of the undisturbed maxima. While this happens the remaining maxima are slightly dragged out of their original position and moved away from the QPCs, which modifies the screening of the saddle potentials and that modulated the total current that passes through the QPCs. On this basis the response pattern of the total current reflects the geometry of the whole undisturbed charge distribution. But also by using a very weak tip potential which is not able to cause such substantial changes in the charge distribution we still get a response according to the original charge distribution. In this way we have demonstrated, that the SGM method has the potential for real space imaging of condensed many particle quantum states.

Acknowledgements:
RAR gratefully acknowledges partial support from EPSRC grant EP/J003476/1.

[1] M. A. Topinka, Science **289**, 2323 (2000)
[2] M. A. Topinka *et al.*, Nature **410**, 183 (2001)
[3] F. Martins *et al.*, Phys. Rev. Lett. **99**, 136807 (2007).
[4] A. Gildemeister *et al.*, Phys. Rev. B **75**, 195338 (2007).
[5] A. Pioda *et al.*, Phys. Rev. B **75**, 045433 (2007).
[6] A. E. Gildemeister *et al.*, Physica E **40**, 1640 (2008).
[7] A. M. Burke *et al.*, Phys. Rev. Lett. **104**, 176801(2010).
[8] S. Schnetz *et al.*, New J. of Phys. **13**, 053013 (2011).
[9] G. A. Steele *et al.*, Phys. Rev. Lett. **95**, 136804. 4 p (2005).
[10] S. Ilani *et al.*, Nature **427**, 328 (2004).
[11] M. G. Pala *et al.*, Phys. Rev. B **77**, 125310 (2008).
[12] M. P. Jura *et al.*, Phys. Rev. B **80**, 041303 (2009).
[13] N. Aoki *et al.*, Phys. Rev. Lett. **108**, 136804 (2012).
[14] Baumgartner A.; Ihn T.; Ensslin K.; et al, **Phys Rev B 76, 085316 (2007)**
[15] Paradiso N. et al, Phys. Rev. B 86, 085326 (2012)
[16] Nicola Paradiso, Stefan Heun et al. Phys. Rev. Lett. **108**, 246801 (2012)
[17] Schnetz S. et al, Phys. Rev. B **82**, 165445 (2010)
[18] Aoki N et al, Phys. Rev. B **77**, 125310 (2008)
[19] Pioda A et al, Physica E **32**, 167-170 (2006)
[20] Gildemeister A.E. et al, Phys. Rev. B **75**, 195338 (2007)
[21] A. A. Kozikov *et al*, arXiv:1401.2370 [cond-mat.mes-hall]
[22] B. Szafran, Phys. Rev. B 84, 075336 (2011)
[23] N. Paradiso et al, Phys. Rev. B 83, 155303 (2011)
[24] A. Baumgartner et al, Phys. Rev. B 74, 165426 (2006)
[25] M.P. Jura et al, Phys. Rev. B 82, 155328 (2010)
[26] R.A. Jalabert et al, Phys. Rev. Lett. 105, 166802 (2010)
[27] E.E. Boyd and R.M. Westervelt, Phys. Rev. B 84, 205308 (2011)
[28] F. Martins, B. Hackens et al, Acta Physica Polonica A 119, 569 (2011)
[29] H Sellier *et al* 2011 *Semicond. Sci. Technol.* **26** 064008 doi:10.1088/0268-1242/26/6/064008
[30] C. Gorini et al, Phys. Rev. B 88, 035406 (2013)
[31] T. Chwiej and B. Szafran, Phys. Rev. B 87, 085302 (2013)
[32] Yang K, Haldane FDM, Rezayi EH, Physical Review B 64, 81301 (2001)
[33] C. Sohrmann and R. A. Römer, phys. stat. sol. (c) **5**, 842 (2008).
[34] C. Sohrmann and R. A. Römer, phys. stat. sol. (b) **245**, 336 (2008)
[35] J. Oswald and M. Oswald, J. Phys.: Cond. Mat. **18**, R101 (2006)
[36] J. Oswald, Int. J. Mod Phys. B **21**, 1424 (2007)
[37] Sohrmann, C., Oswald, J., Römer, R.A.: *Lecture Notes in Physics* **762**, pp. 163-193 (2009)
[38] C. Uiberacker, C. Stecher, J. Oswald: Phys. Rev. B Volume: **86** Issue: **4** Article Number: **045304** (2012)

[39] H. A. Fertig and B. I. Halperin, Phys. Rev. B **36**, 7969 (1987)
[40] N. R. Cooper and J. T. Chalker, Phys. Rev. B **48**, 4530 (1993)
[41] K. Hashimoto *et al.*, Phys. Rev. Lett. **101**, 256802 (2008), arXiv: cond-mat/0807.3784.
[42] C. Sohrmann and R. A. Römer, New J. of Phys. **9**, 97 (2007)